INORGANIC CHEMISTRY FRONTIERS

RESEARCH ARTICLE

View Article Online
View Journal | View Issue

Cite this: *Inorg. Chem. Front.*, 2020, **7**, 3371

A strong zero-phonon line red phosphor $BaNbF_7:Mn^{4+}$ for white LEDs†

Yang Zhou,[a] Xiaoming Wang,*[a] Cuiping Wang,[a] Tian Zhang,[a] Yonggang Wang,[b] Fan Dou[c] and Huan Jiao*[a]

Received 8th May 2020,
Accepted 15th July 2020

DOI: 10.1039/d0qi00522c

rsc.li/frontiers-inorganic

A novel red fluoride phosphor $BaNbF_7:Mn^{4+}$ was synthesized *via* the conventional co-precipitation method. The structure and luminescence properties of $BaNbF_7:Mn^{4+}$ were investigated and discussed under various conditions. The $BaNbF_7:Mn^{4+}$ phosphor shows strong ZPL emission intensity at about 630 nm under ultraviolet (UV) and blue light excitation. It originated from the highly distorted Mn^{4+} octahedral coordination environment in the C_{3v} group symmetry surrounding. A WLED fabricated with a blend of $YAG:Ce^{3+}$ and the $BaNbF_7:Mn^{4+}$ phosphor exhibits a low color temperature (CCT = 3715 K) and a high color rendering index (R_a = 81.2), indicating its potential for application as a red phosphor for WLEDs.

1. Introduction

White light-emitting diodes (WLEDs) have received much attention as next-generation light sources, owing to their low energy consumption, high efficiency and long lifetime.[1–4] Currently, the commercial WLED is obtained by coupling the $Y_3Al_5O_{12}:Ce^{3+}$ ($YAG:Ce^{3+}$) yellow phosphor with a blue-chip (InGaN/GaN).[5–7] However, this type of WLED suffers from the drawbacks of a high correlated color temperature (CCT > 4500 K) and low color rendering index (CRI, R_a < 70), due to the lack of red components, limiting its application range.[8,9] To solve this problem, people are devoted to exploring new red-emitting phosphors. Eu^{2+}-doped nitride and sulfide phosphors have excellent red light-emitting performance.[10–12] However, nitride phosphor synthesis requires harsh synthesis conditions, *e.g.*, high temperature, high atmospheric pressure, and relatively expensive raw materials, which increase the cost of production. Poor chemical stability and moisture sensitivity also restricted sulfide phosphor application in WLEDs. Therefore, it is desirable to explore highly efficient, stable and low-cost red phosphors through a milder synthetic route.

In recent years, narrow-band emission Mn^{4+}-doped red phosphors have attracted lots of attention due to their high luminous efficacy, good thermal stability and low cost. Mn^{4+}-doped fluoride phosphors exhibit strong narrow red emission peaking at 630 nm under UV and blue light excitation. Many Mn^{4+}-doped fluoride phosphors were applied as red components for warm WLEDs. A series of Mn^{4+}-doped fluoride phosphors such as $A_2MF_6:Mn^{4+}$ (A = NH_4^+, K^+, Rb^+, or Cs^+; M = Si^{4+}, Ti^{4+}, Ga^{3+}, Ge^{4+}, Sn^{4+}, or Hf^{4+}),[13–18] $BMF_6:Mn^{4+}$ (B = Ba or Zn; M = Si, Ge, or Ti),[19–21] $A_2BMF_6:Mn^{4+}$ (A/B = Li^+, Na^+, or K^+; M = Al^{3+} or Ga^{3+}),[22–25] and $K_2MF_7:Mn^{4+}$ (M = Ta or Nb)[26] have been reported. Recently, Hu *et al.* successfully synthesized Mn^{4+}-activated oxyfluoride $Na_2WO_2F_4$ with strong ZPL intensity. They claimed that this spectral feature originates from the highly distorted local coordination environment of WO_2F_4 with C_{2v} group symmetry.[27] Fluoride phosphors such as $K_2SiF_6:Mn^{4+}$, *etc.* lack the zero phonon line (ZPL) which is related to the point symmetry of the MnF_6 octahedra with the inversion symmetry.[28,29] When Mn^{4+} local symmetry is distorted to lose the inversion centre, the ZPL emission will be allowed and then possibly dominate the emission spectrum of Mn^{4+}. This feature provides a method to modify the Mn^{4+} emission peak position so that the (oxy)fluoride phosphors can match different application requirements. However, there are very few kinds of Mn^{4+}-doped (oxy)fluoride phosphors that show strong intensity of the ZPL.

In this paper, $BaNbF_7:Mn^{4+}$ phosphor was synthesized based on a conventional co-precipitation method. This phosphor exhibits light pink in daylight and red emission under blue light excitation. We combined a blue LED chip with the $YAG:Ce^{3+}$ yellow phosphor and $BaNbF_7:Mn^{4+}$ red phosphor to make a warm WLED. Low color temperature and high color rendering index values of this WLED device were obtained,

[a]*Key Laboratory of Macromolecular Science of Shaanxi Province, Shaanxi Key Laboratory for Advanced Energy Devices, Shaanxi Engineering Laboratory for Advanced Energy Technology, School of Chemistry & Chemical Engineering, Shaanxi Normal University, Xi'an 710062, Shaanxi Province, P. R. China.*
E-mail: xmwang@snnu.edu.cn, jiaohuan@snnu.edu.cn
[b]*Center for High-Pressure Science and Technology Advanced Research (HPSTAR), Beijing 100094, China*
[c]*Yantai Shield Materials Technology Co., Ltd, Development Zone, Yantai 264006, Shandong Province, P. R. China*

†Electronic supplementary information (ESI) available. CCDC 2001197. For ESI and crystallographic data in CIF or other electronic format see DOI: 10.1039/d0qi00522c

indicating that $BaNbF_7:Mn^{4+}$ is an excellent red phosphor for WLEDs.

2. Experimental section

2.1. Materials and synthesis

The raw materials Nb_2O_5 (99.99%), $Ba(CH_3COO)_2$ (AR), H_2O_2 (30%) and HF (49 wt%) were obtained from Sinopharm Chemical Reagent Co., Ltd. KHF_2 (99.99%) and $KMnO_4$ (99.99%) were obtained from Aladdin Industrial Inc. The $BaNbF_7:Mn^{4+}$ samples were prepared by a co-precipitation method according to the synthetic route illustrated in Fig. 1. A certain amount of Nb_2O_5 was added to a 50 mL Teflon-lined autoclave containing 4 mL of HF solution with stirring for 10 min. The Teflon-lined autoclave was heated at 120 °C for 30 min, and a transparent solution was obtained after the system was cooled down to room temperature. A certain amount of K_2MnF_6 was added into the solution and stirred for 30 minutes. Then a stoichiometric amount of $Ba(CH_3COO)_2$ (aq.) was slowly added into the solution at a dropping speed of 0.2 ml min^{-1} and aged for 24 hours. The resulting pink products were washed with absolute ethanol several times and dried at 60 °C. The pure $BaNbF_7$ phase can be obtained as expressed by the following equation:

$$2Ba(CH_3COO)_2 + Nb_2O_5 + 14HF = 2BaNbF_7 + 4CH_3COOH + 5H_2O \quad (1)$$

2.2. Characterization

Single crystal X-ray diffraction (XRD) data were collected on a Bruker PHOTON II CPAD diffractometer (Cu-Kα radiation) at 293 K by the φ and ω scan mode and reduced using the Crystal Clear Program. The crystal structure of $BaNbF_7$ was solved by a direct method using the SHELXTL™ package of crystallographic software and refined by the full-matrix least-squares technique on F^2.[30,31] The powder XRD data were collected on a Rigaku Mini Flex 600 X-ray powder diffractometer (40 kV, 15 mA, Cu Kα radiation λ = 0.15418 nm) in a continuous scanning mode in the range of 2θ from 10° to 80°. Rietveld refinements of powder XRD data were carried out using the Topas 5.0 software package. The crystal structure of $BaNbF_7$ was optimized by density functional theory (DFT) using the Broyden–Fletcher–Goldfarb–Shanno (BFGS) method.[32] The electronic structure and density of states (DOS) of $BaNbF_7$ were calculated using the Cambridge Serial Total Energy Package (CASTEP)[33] with eigenenergy convergence of self-consistent field (SCF) within 1.0×10^{-7} eV per atom. UV–visible diffuse reflectance spectroscopy (DRS) data of powder samples were collected from 200 to 800 nm on a UV-Vis-NIR spectrophotometer (Shimadzu, UV-3600). The scanning electron microscopy (SEM) images and Energy Dispersive X-ray (EDX) mapping results of samples were obtained using a Philips-FEI Quanta 200 scanning electron microscope equipped with an INCA-Oxford energy-dispersive X-ray spectrometer. The accelerating voltage was set to 10 kV for image capture, and 20 kV for EDX operation. The luminescence properties such as photoluminescence excitation (PLE) spectra, photoluminescence (PL) spectra and temperature-dependent emission spectra were obtained from a Hitachi F-4600 and Edinburgh FLS920 fluorescence spectrophotometer. For the *in situ* high-pressure characterization, standard symmetrical diamond-anvil cells (DACs) were used in all high-pressure measurements. The Mn^{4+}-doped $BaNbF_7$ phosphor was pressed into a pellet and loaded into the sample chamber, which was filled with silicone oil as the pressure transmitting medium (PTM). The pressure was calibrated by adding ruby spheres as the fluorescent pressure indicator. High-pressure Raman experiments were performed in a Renishaw inVia spectrometer using a 532.1 nm excitation laser.

2.3. Fabrication of WLEDs

A WLED device was fabricated with a blue InGaN chip, the commercial yellow phosphor YAG:Ce^{3+}, and the as-synthesized red phosphor $BaNbF_7:Mn^{4+}$. Luminescence properties of the as-fabricated devices were measured under different drive currents from 25 to 350 mA by using an integrating sphere spectroradiometer system (HAAS-1200, Everfine).

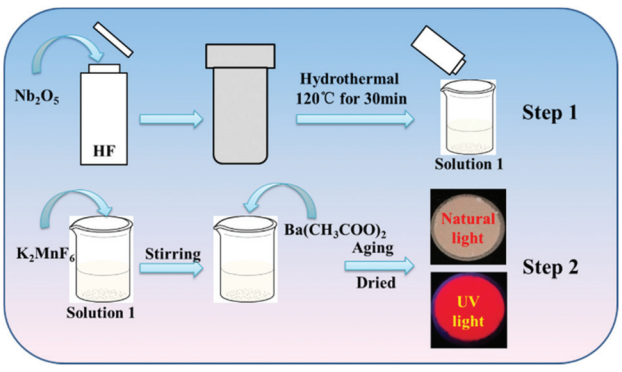

Fig. 1 Schematic of the synthesis process for $BaNbF_7:Mn^{4+}$ by a co-precipitation method.

3. Results and discussion

3.1. Phase identification and structural analysis

A new fluoride $BaNbF_7$ has been prepared *via* the conventional co-precipitation method. The powder XRD pattern of $BaNbF_7$ is the same as that of oxyfluoride $BaNbOF_5$ (JCPDS No. 048-749), which is characterized by X-ray powder diffraction in 1992. However, the single crystal of oxyfluoride $BaNbOF_5$ has not been reported. The crystal structure of $BaNbF_7$ has been analyzed by single-crystal XRD. The typical SEM image of $BaNbF_7$ crystals is shown in Fig. 2. They are in the shape of a cube and has a larger particle size (20–30 μm) with smooth surfaces, clear edges and corners, which implies that this sample has been well crystallized. Single crystal X-ray diffraction reveals that $BaNbF_7$ crystallizes in the cubic space group of $Pa\bar{3}$ (No. 205) and Z = 8 with the unit cell parameters of a =

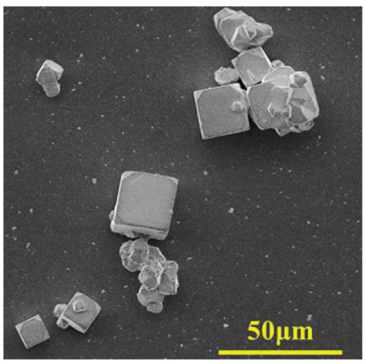

Fig. 2 SEM image of $BaNbF_7$ particles.

9.8855(1) Å and V = 966.0 (5) Å^3. The detailed crystallographic data and structure refinement results are listed in Tables 1 and 2. The atomic displacement parameters, selected bond length and bond angles based on the single crystal data are listed in Tables S1 and S2.† The experimental powder XRD patterns of $BaNbF_7$ and $BaNbF_7$:Mn^{4+} are in good agreement with the simulation results based on the single crystal data (Fig. S1†). The Rietveld refinement of powder XRD data is depicted in Fig. 3a which also shows good fitting residual factors of R_p = 8.29%, R_{wp} = 5.81%, and GOF = 1.18.

Table 1 Crystallographic data for $BaNbF_7$

Composition	$BaNbF_7$
Crystal system	Cubic
Space group	$Pa\bar{3}$ (No. 205)
Lattice parameters (Å)	a = 9.8855 (1)
V (Å^3)	966.0 (5) Å^3
Z	8
Diffractometer	Bruker photon II CPAD
Radiation type	Cu Kα (λ = 1.54178 Å)
Scan mode	φ and ω scans
Temperature (K)	153
Crystal size (mm)	0.03 × 0.03 × 0.03
Crystal color	Clear light colourless
Absorption correction	Multiscan (SADABS)
μ (mm^{-1})	83.46
F (000)	1280
θ range (deg)	$3.9 \leq \theta \leq 34.15$
Indep reflns	227 [R_{int} = 0.079]
Measured reflections	3472
Final R indices [$I > 2\sigma(I)$]	R_1 = 0.0790 wR_2 = 0.0679
R indices(all data)	R_1 = 0.0420 wR_2 = 0.0757
Goodness-of-fit (on F^2)	1.083

Table 2 Crystallographic data of the $BaTaF_7$

Atom	x	y	z	s.o.f.
Ba1	1.00000	0.50000	1.00000	1
Ba2	0.50000	0.00000	0.05000	1
Nb	0.7768(4)	0.2231(6)	0.7231(6)	1
F1	0.6646(4)	0.3354(4)	0.8354(4)	1
F2	0.8999(4)	0.3632(4)	0.7753(4)	1
F3	0.7427(4)	0.0531(5)	0.6168(4)	1

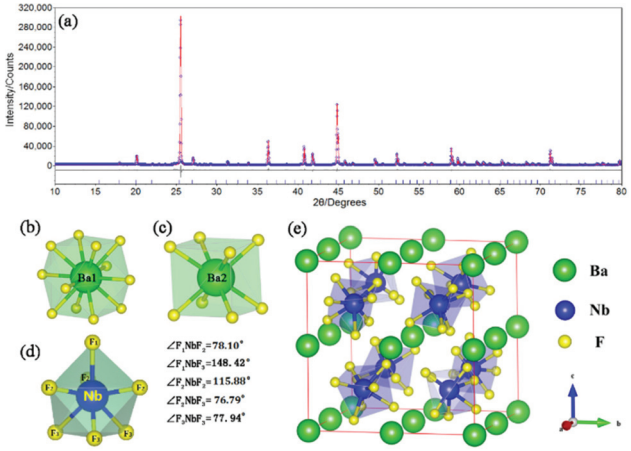

Fig. 3 The Rietveld structure analysis of the red phosphor $BaNbF_7$:Mn^{4+} (a). Coordination sphere of the two different Ba^{2+} sites (b) and (c), and $[NbF_7]$ polyhedra in the crystal structure (d). Crystal structure of $BaNbF_7$ based on the single crystal X-ray diffraction result (e).

The crystal structure of $BaNbF_7$ is depicted in Fig. 3e. The coordination environment surrounding Ba^{2+} cations is shown in Fig. 3b and c; there are two kinds of Ba^{2+} sites with eight and twelve coordination number. The bond length of Ba–F varies from 2.714(5) to 2.842(4) Å. The Nb^{5+} cations are coordinated with seven F^- ions, forming an octahedral coordination geometry with Nb–F distances ranging from 1.914(4) to 2.011(4) Å. Highly distorted $[NbF_7]^{2-}$ polyhedra with C_{3v} group symmetry were interconnected by Ba^{2+} ions in the crystal structure.

3.2. Electronic band structure

The electronic structure calculation of $BaNbF_7$ was performed based on DFT by using the CASTEP module of the Materials Studio package. As shown in Fig. 4a, the top point on the valence band (VB) and the bottom point on the conduction band (CB) are not located at one point, and $BaNbF_7$ possesses an indirect band gap of about 5.14 eV. This means that $BaNbF_7$ is a good luminescent host for Mn^{4+} owing to its wide band gap. The composition of the computed band structures can be further determined from the partial density of states (PDOS) and total density of states (TDOS) diagram (Fig. 4b). The conduction band is mainly composed of the s and p orbitals of Ba and Nb, while F 2p orbitals mainly compose the valence band.

To verify the above theoretical model, the diffuse reflectance spectra (DRS) of the host $BaNbF_7$ and $BaNbF_7$:Mn^{4+} are illustrated in Fig. 4c. The decreasing reflectance of non-doped $BaNbF_7$ (solid blue line) from 200 to 320 nm is ascribed to the host absorption. This spectrum can be further transferred into the energy level to estimate its band gap according to the following equation:

$$(\alpha h\nu)^n = A(h\nu - E_g) \quad (2)$$

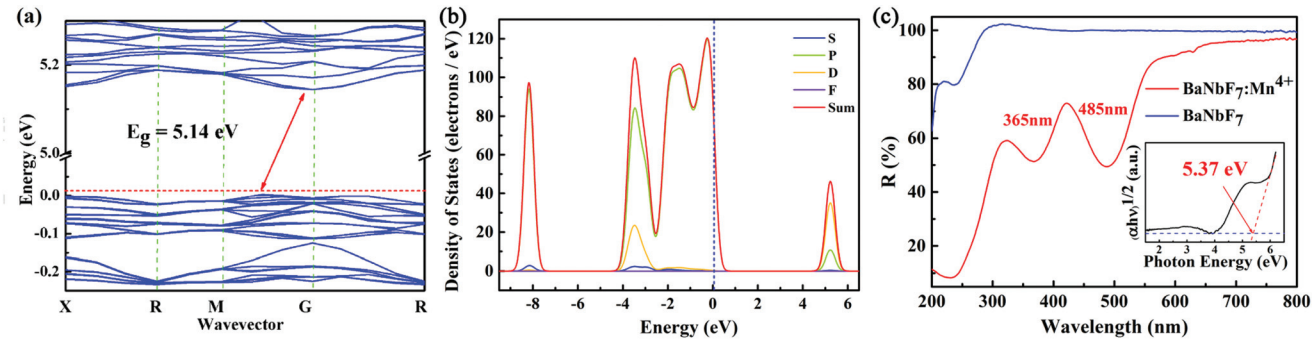

Fig. 4 (a) Calculated energy band structure and (b) the total and partial density of states of $BaNbF_7$. (c) DRS of the $BaNbF_7$ and Mn^{4+}-doped $BaNbF_7$. The inset shows the extrapolation of the band gap energy of $BaNbF_7$.

where $h\nu$ is the photon energy, A is a constant, E_g is the band gap value and α is the absorption coefficient.[31,32] The values of $(\alpha h\nu)^{1/2}$ are plotted as a function of the incident photon energy ($h\nu$) in Fig. 4c. The value of E_g can be extrapolated to be ~5.37 eV. It is similar to the 5.14 eV determined from the DFT calculation. Compared with the non-doped host $BaNbF_7$, the red phosphor $BaNbF_7$:Mn^{4+} (1 mo l%) has two strong absorption bands at about 365 nm and 485 nm, which originate from $^4A_{2g} \rightarrow {}^4T_{1g}$ and $^4A_{2g} \rightarrow {}^4T_{2g}$ spin-allowed transitions of Mn^{4+} ions in the $BaNbF_7$ host lattice, as shown in Fig. 6a and b. Therefore, this phosphor can be effectively excited by blue InGaN chips.

3.3. Morphology and composition analysis

The composition of the as-prepared $BaNbF_7$:Mn^{4+} was investigated by EDX and the corresponding results are shown in Fig. 5a. The elements of Ba, Nb, F and Mn can be easily recognized and the atom ratios of Ba, Nb, and F are about 17.60%, 12.14% and 70.26% respectively, which is close to the ratio of 1 : 1 : 7 in $BaNbF_7$. The SEM image of $BaNbF_7$:Mn^{4+} (1.0 mol%) and the relevant energy dispersive X-ray (EDX) mapping results are shown in Fig. 5b. The Ba, Nb, F, and Mn EDS mapping of the selected area of the sample indicates that Mn^{4+} ions are homogeneously dispersed in the host lattice.

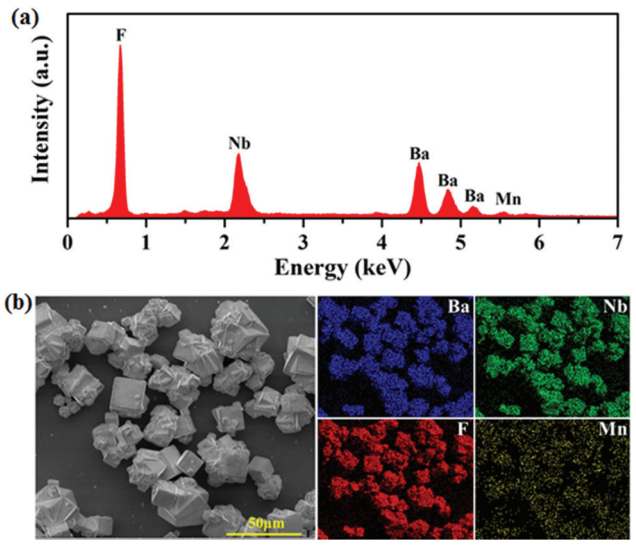

Fig. 5 EDS spectra (a) and typical SEM image and the EDS mapping of the selected area (b) of the $BaNbF_7$:Mn^{4+} (1.0 mol%).

3.4. Luminescence properties and crystal field analyses

The energy level of $3d^n$ ions was calculated by the Tanabe and Sugano theory.[33] The Mn^{4+} T–S energy-level and configurational coordinate diagram of fluoride hosts are depicted in Fig. 6a and b. The luminescence spectrum of Mn^{4+} ions is highly influenced by the distorted $[NbF_7]^{2-}$ polyhedron environment. According to the peak energy at 298 K for the $^2E_g \rightarrow {}^4A_{2g}$ transition of Mn^{4+} (15 873 cm^{-1}), the Racah parameter C is evaluated by the following equation:[34]

$$\frac{E(^2E_g \rightarrow {}^4A_{2g})}{B} = \frac{3.05C}{B} - \frac{1.8B}{D_q} + 7.9 \quad (2)$$

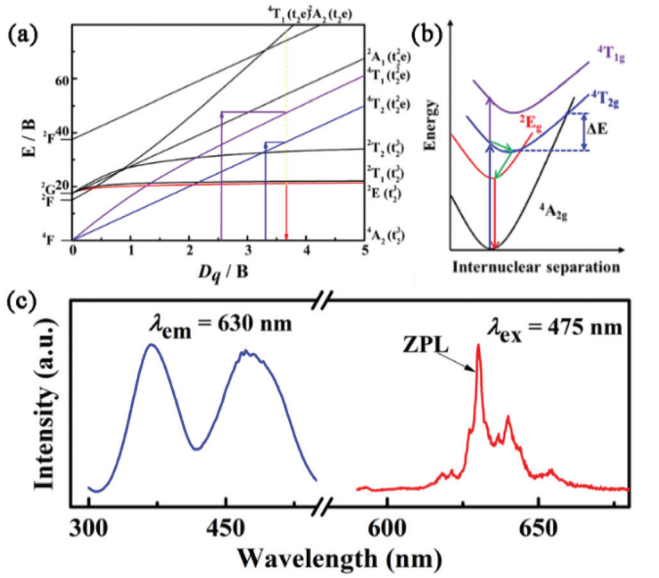

Fig. 6 (a) The Tanabe–Sugano energy-level diagram of Mn^{4+} ions. (b) Configurational coordinate diagram for Mn^{4+} ions in fluoride hosts. (c) Typical PLE and PL spectra of the red phosphor $BaNbF_7$:Mn^{4+}.

The values of D_q, B and C for $BaNbF_7:Mn^{4+}$ are 2105.3, 568.1 and 3838.7 cm^{-1} respectively. Therefore, the ratio of D_q/B is about 3.71. A good red phosphor needs to have strong absorption characteristics in the blue region and the effective emission of red light within 650 nm for blue excited WLEDs. The typical PLE and PL spectra of the red phosphor $BaNbF_7:Mn^{4+}$ obtained at room temperature are presented in Fig. 6c. Two intense excitation bands in PLE spectra located at 368 nm (27 174 cm^{-1}) and 475 nm (21 053 cm^{-1}) can be observed when monitored at 630 nm. Under 475 nm excitation, the phosphor exhibits intense red emission, which can be ascribed to the spin-forbidden $^2E_g \rightarrow {}^4A_{2g}$ transition of Mn^{4+}. The corresponding color coordinates of $BaNbF_7:Mn^{4+}$ were calculated as $x = 0.689$ and $y = 0.311$ based on the emission spectra. The CIE chromaticity diagram of $BaNbF_7:Mn^{4+}$ is shown in Fig. S2.†

The room temperature PL spectra of $BaNbF_7:Mn^{4+}$ red phosphors with various Mn^{4+} concentrations are presented in Fig. 7. As shown in Fig. 7a, the XRD patterns indicate that all the phosphors with Mn^{4+} molar concentrations ranging from 0.5% to 8.0% are all pure phases. The PL spectra of $BaNbF_7:Mn^{4+}$ with different doping concentrations excited under 475 nm are shown in Fig. 7b. The relationship between normalized integrated PL intensity and Mn^{4+} doping concentration is shown in the inset of Fig. 7b. The PL intensity increases firstly and reaches a maximum at a doping concentration of 4.0 mol%, with a continuous increase of Mn^{4+}, and the value gradually decreases due to the concentration quenching.

The phonon–electron interaction is directly related to temperature. At low temperatures, the electrons prefer to distribute in the zero-vibration excited state. When the excited electrons return to the ground state, ZPL and Stokes emissions are released. At high temperatures, electrons prefer to occupy the upper vibrational states which leads to additional anti-Stokes radiation.[15] Fig. 8 presents the temperature-dependent PL spectra of $BaNbF_7:Mn^{4+}$ (77–297 K). There is a slight PL band red-shift when increasing the temperature. It can be explained by the Varshni equation, as shown in Fig. E1 (ESI†).[35] Similar ZPL red-shifts were also observed in the oxyfluoride red phosphor $Na_2WO_2F_4:Mn^{4+}$.[27]

The application of high pressure is an efficient way to change the crystal-field strength and modify the doping site symmetry. In 2015, A. Lazarowska *et al.* reported the pressure effects on the luminescence properties of the red-emitting phosphor $K_2SiF_6:Mn^{4+}$.[36] The PL spectrum of $K_2SiF_6:Mn^{4+}$ consists of several lines attributed to phonon repetitions of the $^2E_g \rightarrow {}^4A_{2g}$ transition and does not contain the ZPL at ambient pressure. When the pressure increased above 9 kbar, the ZPL suddenly appeared, and it remained even after the pressure was removed. They ascribed these changes to pressure-induced local structure transformation of the MnF_6^{2-} octahedron. For the Mn^{4+}-doped K_2SiF_6 [36] and $BaTiF_6$ [37] octahedron structure, the ZPL emission is dependent on the Mn^{4+} ion local symmetry. Any effect that breaks the symmetry under pressure may activate the ZPL. In this work, we tried high pressure to change the crystal-field strength and modify the (Nb/MnF_7) polyhedron symmetry, and then studied the effect of local symmetry on the luminescence of ZPL emission. The red emission of Mn^{4+}-doped $BaNbF_7$ under various pressures is plotted in Fig. 9. When pressure increases, the emission spectra gradually red shift to a longer wavelength from 631.6 nm at 1.6 GPa to 644.2 nm at 20.6 GPa. These red shifts may arise from the decrease of the interelectronic repulsion and the nephelauxetic

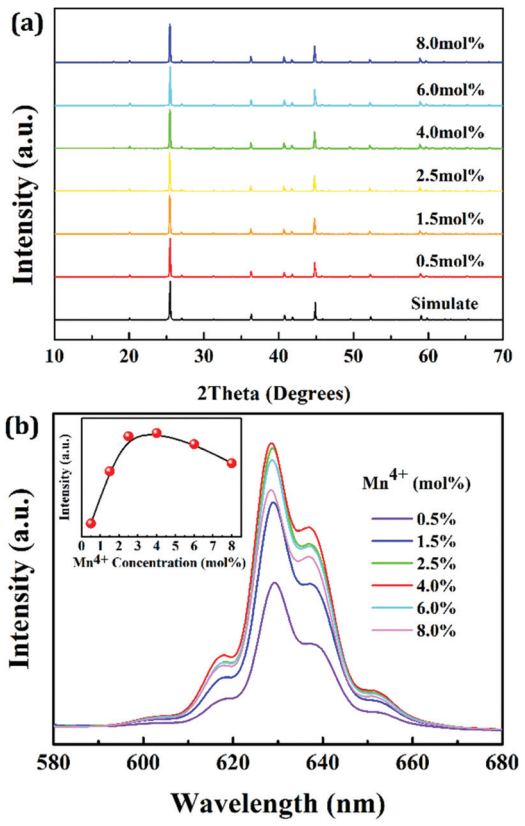

Fig. 7 (a) XRD patterns with different Mn^{4+} concentrations of $BaNbF_7:Mn^{4+}$. (b) PL spectra of $BaNbF_7:Mn^{4+}$ with different doping concentrations. The inset shows the integrating intensity with different Mn^{4+} concentrations.

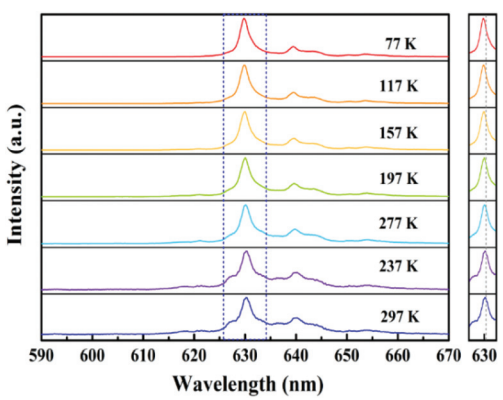

Fig. 8 The temperature-dependent PL spectra of $BaNbF_7:Mn^{4+}$ (77–297 K) under 475 nm excitation.

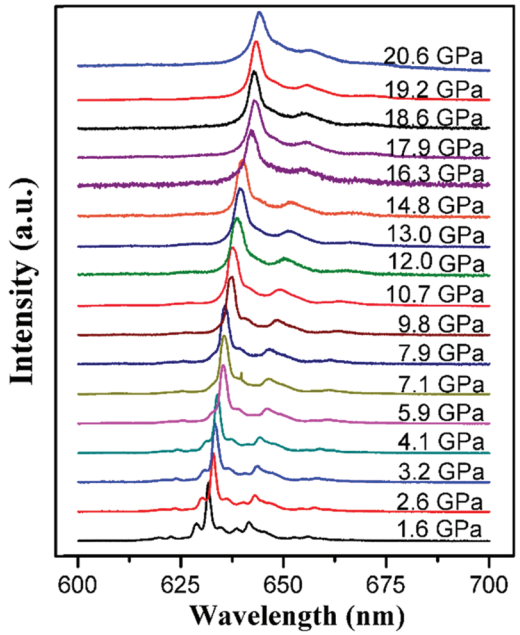

Fig. 9 The emission spectra of Mn^{4+}-doped $BaNbF_7$ as a function of pressure with an excitation laser at a wavelength of 450 nm.

effect which are related to the enhancement of (Nb/Mn–F) bond covalency. Compared with K_2SiF_6 and $BaTiF_6$ octahedra, the $BaNbF_7$ decahedron has a lower symmetry of C_{3v}. When changing the ambient-pressure, C_{3v} group symmetry is likely to rise to a higher point group.

Raman spectroscopy was used to further understand the $BaNbF_7$:Mn^{4+} structural evolution under different pressures. Fig. 10 presents the Raman spectra up to 10.7 GPa at room temperature by using silicone oil as the PTM. At 1.6 GPa, five peaks at wavenumbers 306, 390, 650, 918 and 975 cm^{-1} are observed. When the pressure increases, the vibration peaks shift to a higher wavenumber due to the increase of (Nb/Mn)–F bonding strength. When the pressure reaches 7.1 GPa, the 306 cm^{-1} and 975 cm^{-1} peaks disappear. The number of vibration modes reduced which means that the structure symmetry increased. This Raman result followed the spectrum change. When the pressure increases, $BaNbF_7$:Mn^{4+} rises to a higher symmetry which keeps the ZPL emission not significantly decreased under high pressure.[37]

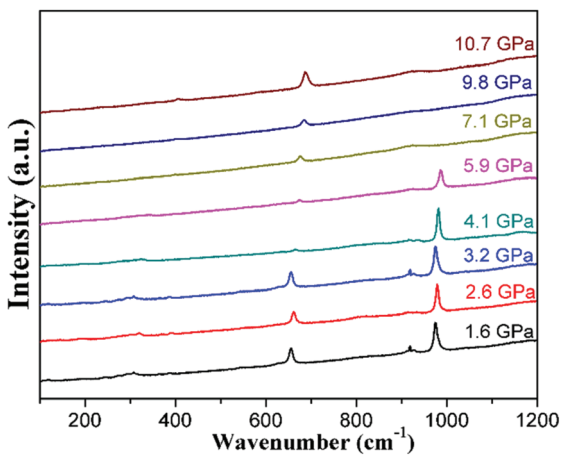

Fig. 10 Raman spectra of Mn^{4+}-doped $BaNbF_7$ at room temperature during compression up to 10.7 GPa.

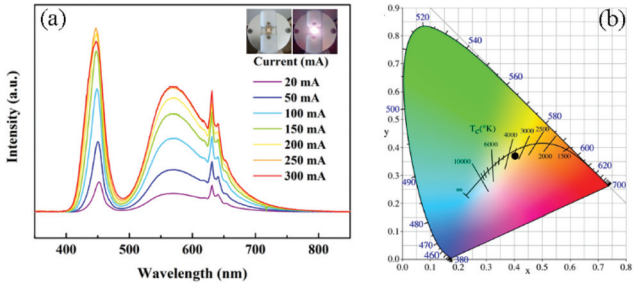

Fig. 11 (a) The EL spectra of a warm WLED against current ranging from 20 to 350 mA. (b) CIE chromaticity diagram of the fabricated white LED at 20 mA.

3.5. Warm LED application

To further evaluate the luminescence characteristics effectively, we fabricated a warm WLED using a blue LED chip combined with the commercially available yellow YAG:Ce^{3+} phosphor and as-synthesized $BaNbF_7$:Mn^{4+} red phosphor. The EL spectra of the warm WLED were recorded under drive currents between 20 and 300 mA as shown in Fig. 11(a). The full spectrum is composed of the three parts. The band shape and peak positions of each part remain constant when the current increases from 20 mA to 350 mA. Besides, the emission intensity increases as the drive current increases. Fig. 11(b) shows the CIE coordinate diagram of the WLED with the color point lying on the black body locus under a drive current of 20 mA. The values of Ra and CCT are 81.2 and 3715 K respectively, indicating the potential of the $BaNbF_7$:Mn^{4+} phosphor as a red component for WLED application.

4. Conclusion

In summary, a new red fluoride phosphor $BaNbF_7$:Mn^{4+} was synthesized by a mild and controllable co-precipitation method. Single-crystal X-ray diffraction reveals that $BaNbF_7$ has a cubic unit cell of a = 9.8855(16) Å and Z = 8 with the $Pa\bar{3}$ space group (No. 205). Mn^{4+} experiences a strong crystal field strength in $BaNbF_7$, with D_q = 2026.9 cm^{-1}, B = 562.1 cm^{-1}, and C = 3838.7 cm^{-1}. Under blue light excitation, Mn^{4+} activated $BaNbF_7$ exhibits a strong ZPL emission at ~630 nm, which originated from the highly distorted Mn^{4+} polyhedron coordination environment. Under different ambient-pressure conditions, the C_{3v} symmetry of $[NbF_7]^{2-}$ is likely to rise to a higher point group. But it didn't cause the ZPL luminescence to significantly change. A WLED device was fabricated with the commercial yellow phosphor YAG:Ce^{3+}, the as-synthesized red

phosphor $BaNbF_7:Mn^{4+}$ and blue InGaN chips. The color rendering index (CRI, R_a = 81.2) and corresponding color temperature (CCT = 3715 K) indicate the potential of the $BaNbF_7:Mn^{4+}$ phosphor as a red component for warm WLED application.

Conflicts of interest

There are no conflicts to declare.

Acknowledgements

This project was funded by the National Natural Science Foundation of China (51972203, 51672167, and 51272151), the Natural Science Foundation of Shaanxi Province (2018JQ5044), and Fundamental Research Funds for the Central Universities (GK202003027).

References

1 E. F. Schubert and J. K. Kim, Solid-state light sources getting smart, *Science*, 2005, **308**, 1274–1278.
2 W. B. Im, N. George, J. Kurzman, S. Brinkley, A. Mikhailovsky, J. Hu, B. F. Chmelka, S. P. DenBaars and R. Seshadri, Efficient and color-tunable oxyfl uoride solid solution phosphors for solid-state white lighting, *Adv. Mater.*, 2011, **23**, 2300–2305.
3 H. Daicho, T. Iwasaki, K. Enomoto, Y. Sasaki, Y. Maeno, Y. Shinomiya, S. Aoyagi, E. Nishibori, M. Sakata, H. Sawa, S. Matsuishi and H. Hosono, A novel phosphor for glareless white light-emitting diodes, *Nat. Commun.*, 2012, **3**, 1132.
4 H. Zhu, C. C. Lin, W. Luo, S. Shu, Z. Liu, Y. Liu, J. Kong, E. Ma, Y. Cao, R.-S. Liu and X. Chen, Highly efficient non-rare-earth red emitting phosphor for warm white light-emitting diodes, *Nat. Commun.*, 2014, **5**, 4312.
5 L. L. Wei, C. C. Lin, Y. Y. Wang, M. H. Fang, H. Jiao and R. S. Liu, Photoluminescent evolution induced by structural transformation through thermal treating in the red narrow-band phosphor K_2GeF_6: Mn^{4+}, *ACS Appl. Mater. Interfaces*, 2015, **7**, 10656–10659.
6 L.-L. Wei, C. C. Lin, M.-H. Fang, M. G. Brik, S.-F. Hu, H. Jiao and R.-S. Liu, A low-temperature co-precipitation approach to synthesize fluoride phosphors K_2MF_6: Mn^{4+} (M = Ge, Si) for white LED applications, *J. Mater. Chem. C*, 2015, **3**, 1655–1660.
7 E. H. Song, J. Q. Wang, S. Ye, X. F. Jiang, M. Y. Peng and Q. Y. Zhang, Room-temperature synthesis and warm-white LED applications of Mn^{4+} ion doped fluoroaluminate red phosphor Na_3AlF_6: Mn^{4+}, *J. Mater. Chem. C*, 2016, **4**, 2480–2487.
8 Y. Jin, M.-H. Fang, M. Grinberg, S. Mahlik, T. Lesniewski, M. G. Brik, G.-Y. Luo, J. G. Lin and R.-S. Liu, Narrow red emission band fluoride phosphor $KNaSiF_6$: Mn^{4+} for warm white light-emitting diodes, *ACS Appl. Mater. Interfaces*, 2016, **8**, 11194–11203.
9 T. T. Deng, E. H. Song, J. Sun, L. Y. Wang, Y. Deng, S. Ye, J. Wang and Q. Y. Zhang, The design and preparation of the thermally stable, Mn^{4+} ion activated, narrow band, red emitting fluoride Na_3GaF_6: Mn^{4+} for warm WLED applications, *J. Mater. Chem. C*, 2017, **5**, 2910–2918.
10 H.-D. Nguyen and R.-S. Liu, Narrow-band red-emitting Mn^{4+}-doped hexafluoride phosphors: synthesis, optoelectronic properties, and applications in white light-emitting diodes, *J. Mater. Chem. C*, 2016, **4**, 10759–10775.
11 X. Piao, K.-I. Machida, T. Horikawa, H. Hanzawa, Y. Shimomura and N. Kijima, Preparation of $CaAlSiN_3$: Eu^{2+} phosphors by the self-propagating high-temperature synthesis and their luminescent properties, *Chem. Mater.*, 2007, **19**, 4592–4599.
12 K. Uheda, N. Hirosaki, Y. Yamamoto, A. Naito, T. Nakajima and H. Yamamoto, Luminescence properties of a red phosphor, $CaAlSiN_3$: Eu^{2+} for white light-emitting diodes, *Electrochem. Solid-State Lett.*, 2006, **9**, H22–H25.
13 Q. Zhou, Y. Zhou, Y. Liu, Z. Wang, G. Chen, J. Peng, J. Yan and M. Wu, A new and efficient red phosphor for solid-state lighting: Cs_2TiF_6: Mn^{4+}, *J. Mater. Chem. C*, 2015, **3**, 9615–9619.
14 F. Tang, Z. Su, H. Ye, M. Wang, X. Lan, D. L. Phillips, Y. Cao and S. Xu, A set of manganese ion activated fluoride phosphors ($A_2BF_6:Mn^{4+}$, A = K, Na, B = Si, Ge, Ti): synthesis below 0 °C and efficient room-temperature photoluminescence, *J. Mater. Chem. C*, 2016, **4**, 9561–9568.
15 W.-L. Wu, M.-H. Fang, W. Zhou, T. Lesniewski, S. Mahlik, M. Grinberg, M. G. Brik, H.-S. Sheu, B.-M. Cheng, J. Wang and R.-S. Liu, High color rendering index of $Rb_2GeF_6:Mn^{4+}$ for light-emitting diodes, *Chem. Mater.*, 2017, **29**, 935–939.
16 Q. Zhou, Y. Zhou, Y. Liu, L. Luo, Z. Wang, J. Peng, J. Yan and M. Wu, A new red phosphor $BaGeF_6:Mn^{4+}$: hydrothermal synthesis, photo-luminescence properties, and its application in warm white LED devices, *J. Mater. Chem. C*, 2015, **3**, 3055–3059.
17 J. S. Zhong, D. Q. Chen, X. Wang, L. F. Chen, H. Yu, Z. G. Ji and W. D. Xiang, Synthesis and optical performance of a new red-emitting $ZnTiF_6{\cdot}6H_2O$: Mn^{4+} phosphor for warm white-light-emitting diodes, *J. Alloys Compd.*, 2016, **662**, 232–239.
18 R. Hoshino and S. Adachi, Optical spectroscopy and degradation behavior of $ZnGeF_6{\cdot}6H_2O$: Mn^{4+} red-emittingphosphor, *J. Lumin.*, 2015, **162**, 63–71.
19 T. T. Deng, E. H. Song, Y. Y. Zhou, L. Y. Wang, S. Ye and Q. Y. Zhang, Stable narrow-band red phosphor K_3GaF_6: Mn^{4+} derived from hydrous $K_2GaF_5(H_2O)$ and K_2MnF_6, *J. Mater. Chem. C*, 2017, **5**, 9588–9596.
20 E. Song, J. Wang, J. Shi, T. Deng, S. Ye, M. Peng, J. Wang, L. Wondraczek and Q. Zhang, Highly efficient and thermally stable K_3AlF_6: Mn^{4+} as a red phosphor for ultra-high-performance warm white light-emitting diodes, *ACS Appl. Mater. Interfaces*, 2017, **9**, 8805–8812.
21 H. Lin, T. Hu, Q. Huang, Y. Cheng, B. Wang, J. Xu, J. Wang and Y. Wang, Non-rare-earth $K_2XF_7:Mn^{4+}$ (X = Ta, Nb): a highly-efficient narrow-band red phosphor enabling the

application in wide-color-gamut LCD, *Laser Photonics Rev.*, 2017, **11**, 1700148.

22 L. Y. Wang, E. H. Song, T. T. Deng, Y. Y. Zhou, Z. F. Liao, W. R. Zhao, B. Zhou and Q. Y. Zhang, Luminescence properties and warm white LED application of a ternary-alkaline fluoride red phosphor K_2NaAlF_6:Mn^{4+}, *Dalton Trans.*, 2017, **46**, 9925–9933.

23 E. Song, J. Wang, J. Shi, T. Deng, S. Ye, M. Peng, J. Wang, L. Wondraczek and Q. Zhang, Highly efficient and thermally stable K_3AlF_6: Mn^{4+} as a red phosphor for ultra-high-performance warm white light-emitting diodes, *ACS Appl. Mater. Interfaces*, 2017, **9**, 8805–8812.

24 S. Qiu, H. Wei, M. Wang, S. Zhang, Y. Zhou, L. Xu, X. Wang and H. Jiao, Synthesis and photoluminescence of Mn^{4+} activated ternary-alkaline fluoride K_2NaGaF_6 red phosphor for warm-white LED application, *RSC Adv.*, 2017, **7**, 50396–50402.

25 Y. Jin, M.-H. Fang, M. Grinberg, S. Mahlik, T. Lesniewski, M. G. Brik, G.-Y. Luo, J. G. Lin and R.-S. Liu, Narrow red emission band fluoride phosphor $KNaSiF_6$: Mn^{4+} for warm white light-emitting diodes, *ACS Appl. Mater. Interfaces*, 2016, **8**, 11194–11203.

26 T. Jansen, F. Baur and T. Justel, Red emitting K_2NbF_7: Mn^{4+} and K_2TaF_7: Mn^{4+} for warm-white LED applications, *J. Lumin.*, 2017, **192**, 644–652.

27 T. Hu, H. Lin, Y. Cheng, Q. M. Huang, J. Xu, Y. Gao, J. M. Wang and Y. S. Wang, A highly-distorted octahedron with a C-2v group symmetry inducing an ultra-intense zero phonon line in Mn4+-activated oxyfluoride $Na_2WO_2F_4$, *J. Mater. Chem. C*, 2017, **5**, 10524–10532.

28 L. Huang, Y. Zhu, X. Zhang, R. Zou, F. Pan, J. Wang and M. Wu, HF-free hydrothermal route for synthesis of highly efficient narrow-band red emitting phosphor $K_2Si_{1-x}F_6$: xMn^{4+} for warm white light-emitting diodes, *Chem. Mater.*, 2016, **28**, 1495–1502.

29 L. Huang, Y. Liu, J. Yu, Y. Zhu, F. Pan, T. Xuan, M. G. Brik, C. Wang and J. Wang, Highly stable K_2SiF_6: Mn^{4+}@K_2SiF_6 composite phosphor with narrow red emission for white LEDs, *ACS Appl. Mater. Interfaces*, 2018, **10**, 18082–18092.

30 G. M. Sheldrick, *SHELXS97, Program for crystal structure solution*, Germany, 1997.

31 G. M. Sheldrick, A short history of SHELX, *Acta Crystallogr., Sect. A: Found. Crystallogr.*, 2008, **64**, 112–122.

32 J. Nocedal, Updating quasi-newton matrices with limited storage, *J. Math. Comput.*, 1980, **35**, 773–782.

33 M. D. Segall, P. J. D. Lindan, M. J. Probert, C. J. Pickard, P. J. Hasnip, S. J. Clark and M. C. Payne, First-principles simulation: ideas, illustrations and the CASTEP code, *J. Phys.: Condens. Matter*, 2002, **14**, 2717–2744.

34 B. Henderson and G. F. Imbusch, *Optical spectroscopy of inorganic solids*, Oxford University Press, 2006.

35 Y. P. Varshni, Temperature dependence of the energy gap in semiconductors, *Physica*, 1967, **34**, 149–154.

36 A. Lazarowska, S. Mahlik, M. Grinberg, C. C. Lin and R. S. Liu, Pressure effect on the zero-phonon line emission of Mn4+ in K_2SiF_6, *J. Chem. Phys.*, 2015, **143**, 134704.

37 Y. G. Wang, T. Wen, L. Y. Tang, L. X. Yang, W. G. Yang and Y. S. Zhao, Impact of hydrostatic pressure on the crystal structure and photoluminescence properties of Mn^{4+}-doped $BaTiF_6$ red phosphor, *Dalton Trans.*, 2015, **44**, 7578–7585.

